On Friction Regimes in Quantitative Elastohydrodynamics

W. Habchi[1,2*], S. Bair[2] and P. Vergne[3]

[1] Lebanese American University, Dep. of Ind. & Mech. Eng., Byblos, Lebanon
[2] G.W. Woodruff School of Mech. Eng., Center for High Pressure Rheology, Georgia Institute of Technology, Atlanta, GA 30332-0405
[3] Université de Lyon, CNRS, INSA-Lyon, LaMCoS UMR5259, F-69621, France

*At the time this work was done, the first author was holding a visiting scholar position at Georgia Institute of Technology

Abstract

This paper identifies the different friction regimes encountered in elastohydrodynamic lubricated point contacts using a quantitative, physics-based approach. The idea is to link different traction regimes to dimensionless numbers and identify ranges of those numbers where a given regime is encountered or dominates the friction response of the contact. A numerical investigation of traction in point contacts lubricated with a typical mineral oil is employed. The measured thermo-physical properties of the oil are used without any modification to force agreement with experiments. The authors propose four friction regimes delimited by the combined values of three dimensionless parameters.

Keywords: elastohydrodynamic lubrication, traction regimes, dimensionless numbers

1. Introduction

Lubrication has been a topic of interest for the engineering community during the last century. In particular, elastohydrodynamic lubrication (EHL) has gained much attention since its recognition as the main physical mechanism behind the successful operation of important mechanical elements such as roller bearings and transmission gears. Ever since the first theoretical studies, researchers faced major difficulties in matching the theoretical performance of elastohydrodynamic (EHD) contacts with the measured performance. Early on, both film thickness and friction predictions failed to agree with experiments unless the lubricant properties were treated as adjustable parameters. This was not a shortcoming of the employed theoretical / numerical tools that were employed. It was rather due to the use of inappropriate rheological models that failed to describe the thermophysical properties of lubricants under the severe conditions encountered in EHD contacts. Tribology has come a long way since then and film thicknesses can be predicted with a fairly good accuracy nowadays. This is because the tribological community began to employ more realistic rheological models that are better capable of capturing the dependence of the lubricant transport properties on pressure, temperature and shear stress at least up to a few hundred MPa. It is well known that the lubricant film thickness in EHL contacts depends mainly on the rheological behavior of the lubricant in the inlet area of the

contact where pressure remains relatively low. As for friction, it is well known that frictional behavior of EHL contacts greatly depends on the rheological behavior of the lubricant in the central high pressure area of the contact. In the latter, pressures can go as high as 1-3 GPa with extremely high shear rates associated with important thermal dissipation. This makes the situation much more difficult, and the rheological behavior of lubricants under such conditions has been poorly known. Moreover, the classical rheological models that have been used in EHL theoretical studies drastically fail to represent real rheological behavior, leading to an important gap between theoretical predictions of friction and experiments. To overcome this, until recently, the trend has been to retain the classical rheological models while altering their parameters without regard to sound theory or accurate measurements in order to achieve a reasonable agreement with experiments. Obviously this approach failed to yield any reasonable understanding of the contribution of liquid properties to the contact frictional response.

Interest in understanding EHL traction has a long history. In 1960, Smith [1], in offering an explanation of the limited friction coefficients in full-films, first speculated that a liquid must possess a limit to the shear stress. Crook [2], in 1963 proposed a viscoelastic model in which the liquid had an effective viscosity which decreased with rolling speed and increased with pressure rapidly at low pressures and slowly at high pressures. About the same time, Bell [3] proposed that a non-Newtonian sinh-law could explain the discrepancies between measured film thickness and friction and the Newtonian calculations. Johnson and Tevaarwerk [4] and Hirst and Moore [5] continued this line of reasoning for the explanation to traction in full films; however, Johnson and Tevaarwerk also found that in some cases the limiting stress concept was useful. More recently, an attempt was made to generate a universal traction curve [6]. One clear shortcoming of these approaches was the inability to make use of the viscosity that could be measured in a viscometer.

Only recently, there has been a growing interest for including more realistic, physics-based rheological models [7] [8] in theoretical EHL predictions [9][10][11]. In [12], the authors used the actual measured transport properties of a typical mineral oil (Shell T9) to derive appropriate rheological models representing the pressure, temperature, and shear stress dependence of viscosity including the limiting-shear-stress behavior, in addition to the pressure-temperature dependence of the density and the thermal properties (thermal conductivity and heat capacity). The developed models were used without any alteration of their corresponding parameters, in a numerical model to predict the frictional behavior of EHL point contacts under a wide range of operating conditions. The predicted results showed excellent agreement with experiments, allowing the authors to establish in a more recent work a thorough investigation of the contribution of the actual lubricant properties inside the contact to the frictional behavior of these contacts. For more details, the interested reader is referred to [13]. Hence, a validated framework for the theoretical prediction of friction in EHL contacts was established.

In this work, the authors use the previously developed framework to run an extensive numerical test campaign for the determination of traction / friction curves for the Shell T9 lubricant under a wide range of operating conditions. The purpose is to identify different friction regimes encountered in EHL contacts and linking these regimes to some dimensionless numbers. The idea is to identify the ranges of the proposed dimensionless numbers where each regime is encountered or dominates the frictional response of the contact. In having a quantitative, physics-based approach this work differs from most other investigations of regimes of EHL traction, for example [14]. It will become apparent that the delineation of various regimes of traction behavior is quite complex and requires knowledge of the thermophysical properties of the liquid and that the previous attempts at delineating regimes by visual inspection of traction curves could not achieve success.

2. Lubricant Thermophysical Properties

The thermophysical properties of lubricant Shell T9 were discussed in detail in [12]. The variations of these properties with pressure, temperature and shear stress were measured and appropriate models were derived to represent these variations. The derived models are briefly recalled in the following. For further details, the interested reader is referred to [12] and references therein. Subscripts 0 and R indicate, respectively, ambient pressure and temperature ($p_0 = 0$ and $T_0 = 30^o\mathrm{C}$) and a reference state ($p_R = 0$ and $T_R = 25^o\mathrm{C}$).

2.1 Density

The Murnaghan [15] equation of state is used to model the density variation of lubricant Shell T9 with pressure p and temperature T:

$$\rho = \frac{\rho_R}{1 + a_V\left(T - T_R\right)} \times \left(1 + \frac{K_0'}{K_0}\, p\right)^{\frac{1}{K_0'}} \quad \text{with} \quad K_0 = K_{00}\exp\left(-\beta_K T\right) \qquad (1)$$

Where $K_0' = 10.545$, $a_V = 7.734\times10^{-4}\ \mathrm{K}^{-1}$, $K_{00} = 9.234\ \mathrm{GPa}$, $\rho_R = 875\,Kg/m^3$ and $\beta_K = 6.090\times10^{-3}\ \mathrm{K}^{-1}$ were obtained from experimental measurement.

2.2 Viscosity

A Vogel-like model [7] [16] with a thermodynamic scaling parameter is used to represent the pressure and temperature dependence of the limiting low-shear viscosity of Shell T9 mineral oil:

$$\mu = \mu_\infty \exp\left(\frac{B_F\varphi_\infty}{\varphi - \varphi_\infty}\right) \quad \text{with} \quad \varphi = \left(\frac{T}{T_R}\right)\left(\frac{V}{V_R}\right)^g \qquad (2)$$

Where $g = 5.0348$, $\varphi_\infty = 0.26844$, $B_F = 12.898$, and $\mu_\infty = 1.489 \times 10^{-4}$ Pa·s were obtained from experimental measurement. And from the Murnaghan equation of state:

$$\frac{V}{V_R} = \frac{1 + a_V \left(T - T_R\right)}{\left(1 + \frac{K_0'}{K_0} p\right)^{1/K_0'}} \qquad (3)$$

As for the shear dependence of viscosity, the single-Newtonian modified Carreau-Yasuda equation [17] is used to define the generalized viscosity η as a function of shear stress τ as follows:

$$\eta = \frac{\mu}{\left[1 + \left(\frac{\tau}{G}\right)^a\right]^{\frac{\frac{1}{n} - 1}{a}}} \qquad (4)$$

Where $G = 7.0$ MPa, $a = 5$ and $n = 0.35$ were obtained from experimental measurements. Finally, Shell T9 lubricant was shown to exhibit a limiting shear stress behavior under high shear rates. The limiting value of the shear stress τ_L was shown to depend on pressure according to:

$$\tau_L = \Lambda \, p \qquad (5)$$

Where the limiting stress-pressure coefficient $\Lambda = 0.083$. This value was deduced from EHL traction experiments carried out under isothermal operating conditions.

2.3 Thermal Conductivity

The thermal conductivity k of Shell T9 was also obtained from experimental transient hot-wire measurements [12] and its variation with temperature and pressure was represented by the following equation:

$$k = B_k + C_k \kappa^{-s} \quad \text{with} \quad \kappa = \left(\frac{V}{V_R}\right)\left[1 + A\left(\frac{T}{T_R}\right)\left(\frac{V}{V_R}\right)^3\right] \qquad (6)$$

Where $A = -0.101$, $B_k = 0.053\ \mathrm{W/m \cdot K}$, $C_k = 0.026\ \mathrm{W/m \cdot K}$ and $s = 7.6$ were obtained from experimental measurements. The term V/V_R is obtained from equation (3).

2.4 Volumetric Heat Capacity

Finally, the volumetric heat capacity $C = \rho c$ of Shell T9 was measured [12] and its pressure-temperature dependence was represented by the following model:

$$C = C' + m\chi \qquad \text{with} \qquad \chi = \left(\frac{T}{T_R}\right)\left(\frac{V}{V_R}\right)^{-4} \qquad (7)$$

Where $C' = 1.17\times10^{6}\ J/m^3\cdot K$ and $m = 0.39\times10^{6}$ J/m$^3\cdot$K were obtained from experimental transient hot-wire measurements. Again, the term V/V_R is obtained from equation (3).

3. Numerical Model Description

A detailed description of the numerical model used in this work can be found in [11] and [18]. In this section only a brief reminder of the main features of this model is provided. This model is based on a Full-System Finite Element resolution procedure. The generalized Reynolds, linear elasticity and load balance equations define the EHL part of the model. The Reynolds equation for a steady-state point contact between a ball and a flat plane lubricated with a generalized Newtonian lubricant under unidirectional surface velocities in the x-direction is given by Yang and Wen [19]:

$$\frac{\partial}{\partial x}\left[\left(\frac{\rho}{\eta}\right)_e h^3\frac{\partial p}{\partial x}\right] + \frac{\partial}{\partial y}\left[\left(\frac{\rho}{\eta}\right)_e h^3\frac{\partial p}{\partial y}\right] = 12\frac{\partial}{\partial x}\left(\rho^* U_m h\right) \qquad (8)$$

Where:

$$U_m = \frac{u_p + u_s}{2} \qquad \left(\frac{\rho}{\eta}\right)_e = 12\left(\frac{\eta_e\rho'_e}{\eta'_e} - \rho''_e\right)$$

$$\rho^* = \frac{\left[\rho'_e\eta_e\left(u_s - u_p\right) + \rho_e u_p\right]}{U_m} \qquad \rho_e = \frac{1}{h}\int_0^h \rho\, dz$$

$$\rho'_e = \frac{1}{h^2}\int_0^h \rho \int_0^z \frac{dz'}{\eta} dz \qquad \rho''_e = \frac{1}{h^3}\int_0^h \rho \int_0^z \frac{z'dz'}{\eta} dz$$

$$\frac{1}{\eta_e} = \frac{1}{h}\int_0^h \frac{dz}{\eta} \qquad \frac{1}{\eta'_e} = \frac{1}{h^2}\int_0^h \frac{z\,dz}{\eta}$$

Note that this equation accounts for the variations of both density and viscosity across the film thickness through the integral terms. In fact, the changes in density are due to temperature variations across the lubricant film whereas the changes in viscosity stem from both temperature and shear rate variations across the film. Moreover, both density and viscosity are allowed to vary with pressure and temperature throughout the lubricant film. Indices *p* and *s* correspond to the plane and the sphere respectively and η is the generalized Newtonian viscosity. The film thickness *h* in equation (8) is replaced by:

$$h(x,y) = h_0 + \frac{x^2+y^2}{2R} - \delta(x,y) \qquad (9)$$

Where R is the radius of the ball and $\delta(x,y)$ corresponds to the normal elastic deformation of the solid surfaces at every point (x,y) of the two-dimensional contact area Ω_c. It is obtained by solving the linear elasticity equations on a large *3D* solid body representing a half-space domain. To complete the EHL part, the load balance equation is used to monitor the value of the rigid body displacement h_0 and ensure that the correct external load F is applied to the contact. This equation reads:

$$\int_{\Omega_c} p \, d\Omega = F \qquad (10)$$

As for the thermal part, the temperature distribution in the two solid bodies and the lubricant film is obtained by solving the *3D* energy equation. For the solid parts p and s this equation reads:

$$\begin{cases} c_p \rho_p u_p \dfrac{\partial T}{\partial x} = k_p \left(\dfrac{\partial^2 T}{\partial x^2} + \dfrac{\partial^2 T}{\partial y^2} + \dfrac{\partial^2 T}{\partial z^2} \right) \\ c_s \rho_s u_s \dfrac{\partial T}{\partial x} = k_s \left(\dfrac{\partial^2 T}{\partial x^2} + \dfrac{\partial^2 T}{\partial y^2} + \dfrac{\partial^2 T}{\partial z^2} \right) \end{cases} \qquad (11)$$

The geometrical domains of solids p and s are taken as infinite layers with a finite thickness sufficiently large to have zero temperature gradient away from the contact area. As for the lubricant film, the energy equation is given by:

$$\rho c \left(u_f \frac{\partial T}{\partial x} + v_f \frac{\partial T}{\partial y} \right) = k \frac{\partial^2 T}{\partial z^2} - \frac{T}{\rho} \frac{\partial \rho}{\partial T} \left(u_f \frac{\partial p}{\partial x} + v_f \frac{\partial p}{\partial y} \right) + \eta \left[\left(\frac{\partial u_f}{\partial z} \right)^2 + \left(\frac{\partial v_f}{\partial z} \right)^2 \right] \qquad (12)$$

Where the lubricant velocity field components u_f and v_f in the x and y directions respectively are given by:

$$\begin{aligned} u_f &= u_p + \frac{\partial p}{\partial x} \left[\int_0^z \frac{z' dz'}{\eta} - \frac{\eta_e}{\eta'_e} h \int_0^z \frac{dz'}{\eta} \right] + \frac{\eta_e (u_s - u_p)}{h} \int_0^z \frac{dz'}{\eta} \\ v_f &= \frac{\partial p}{\partial y} \left[\int_0^z \frac{z' dz'}{\eta} - \frac{\eta_e}{\eta'_e} h \int_0^z \frac{dz'}{\eta} \right] \end{aligned} \qquad (13)$$

Equations (8-13) completely define the thermal EHL problem. These equations are solved using the usual EHL boundary conditions. That is, for the generalized Reynolds equation zero pressure is assumed on the boundary of the contact area Ω_c and the free boundary problem arising at the exit of the contact is handled by applying the penalty method [20]. As for the linear elasticity part, the pressure distribution obtained from Reynolds equation is used as a normal

pressure load boundary condition on the contact surface Ω_c. Finally, for the thermal part, an ambient temperature T_0 boundary condition is applied at the inlet of the solid bodies and the lubricant film and a continuity boundary condition is applied at the two lubricant-solid interfaces. All equations discretized using a finite element approximation and solved in dimensionless form. Non-structured meshing is used throughout the different parts of the problem. For the hydrodynamic part (generalized Reynolds equation), fifth order Lagrange triangular elements (2D) are employed whereas for the elastic part Lagrange second order tetrahedral elements (3D) are used. Using higher order elements for the hydrodynamic problem, as an alternative to refining the mesh, allows having a good precision for its solution without inducing any unnecessary increase in the number of degrees of freedom in the three-dimensional elastic problem. For the thermal part, Lagrange second order tetrahedral elements are also employed. The meshing of all geometric components is tailored towards the nature of the EHL problem. That is, the mesh is always finer in the central area of the contact where additional precision is required owing to the sharper solution gradients that are encountered. For more details regarding the geometry and its meshing, the reader is referred to [18].

The global numerical procedure consists in starting with an initial guess for pressure, film thickness and temperature. The generalized Reynolds, linear elasticity and load balance equations are solved simultaneously using a damped Newton resolution [21]. The resulting pressure and film thickness distributions are then used to solve the thermal problem defined by equations (11-13) which are also solved simultaneously. An iterative procedure is thus established between the respective solutions of the EHL and thermal problems. This iterative procedure is repeated until the pressure and temperature solutions are converged, that is until the maximum absolute difference between the pressure solutions and the maximum relative difference between the temperature solutions at two consecutive resolutions falls below 10^{-3}. Throughout the iterative procedure, every time the shear stress τ is evaluated (using viscosity data provided by a combination of the Carreau and Vogel-like models) it is either truncated to τ_L if it exceeds τ_L or, otherwise, it is kept unchanged. Note that for highly loaded contacts, special stabilized finite element formulations are needed for the solution of the generalized Reynolds equation. Similar formulations are also needed for the solution of the energy equations in a convection-dominated regime. For more details about these stabilized formulations, the convergence criteria, the definition of the penalty term for the treatment of the free boundary problem and the numerical precision of this solution scheme the reader is referred to [18].

It is noteworthy to mention that, in this model, the dependence of the transport properties of the lubricant on pressure, temperature and shear stress is fully incorporated as described by the thermophysical models of the previous section. The importance of including all these dependencies in any numerical model for an accurate prediction of friction has been thoroughly discussed in [12] and [13]. In the current work, and in order to clearly reveal the different traction regimes encountered in EHL contacts, four different sets of numerical tests are run:

1- **Full Potential:** the full potential of the numerical model is considered. That is, thermal dissipation inside the contact is taken into account along with the shear-thinning behavior of the lubricant as described by equation (4) and the Limiting Shear Stress (LSS) behavior as described by equation (5).

2- **Thermal Off:** thermal effects are switched off. That is, isothermal conditions are assumed.

3- **LSS Off:** the Limiting Shear Stress behavior of the lubricant is switched off. That is the shear stress inside the lubricant film is allowed to increase indefinitely.

4- **Shear-Thinning Off:** the shear-thinning behavior of the lubricant is switched off. In other words, the lubricant is assumed to have Newtonian behavior.

Note that for the last three, only one physical parameter is switched off while all the remainder remains included e.g. for the "Thermal Off" cases, thermal effects are turned off whereas shear-thinning and limiting shear stress effects are included. These four sets will help clearly identify when each physical parameter begins to affect friction, or even when it dominates the frictional behavior of the contact.

4. Representative Dimensionless Numbers

In this section, a set of well-known dimensionless numbers is recalled. In addition, new dimensionless numbers are developed to help predict the importance of limiting shear stress and roller compliance. All the dimensionless numbers discussed in this section shall be used later to quantitatively delineate traction regimes in EHL contacts.

4.1 Weissenberg Number

The Weissenberg number [22] is a well-known dimensionless number in rheology. It is defined as $Wi = \lambda\dot{\gamma}$, where λ is a characteristic time parameter and $\dot{\gamma}$ corresponds to shear rate. The value of the characteristic time λ, is $\lambda = \mu/G \approx \mu M/\rho R_g T$ where M is molecular weight, μ is the low-shear viscosity, ρ is mass density and R_g is the universal gas constant. Therefore the Weissenberg number can also be written as:

$$Wi = \frac{\tau}{G} \qquad (14)$$

Shear-thinning can be said to occur for a given liquid when the Weissenberg number becomes greater than unity. In this work, the Weissenberg number will be evaluated at the contact center.

4.2 Nahme-Griffith Number

The Nahme-Griffith number [23] is another well-known dimensionless number in Rheology. It characterizes thermal feedback for a plane Couette flow of thickness *h*:

$$Na = \frac{\beta \tau^2 h^2}{k\mu} = \frac{\beta \mu \dot{\gamma}^2 h^2}{k} = \frac{\beta \mu \left(V_1 - V_2\right)^2}{k} \qquad (15)$$

where $\beta = -\partial \ln \mu / \partial T$, V_1 and V_2 are the surface velocities of the contacting solids. For $Na > 1$ the viscous dissipation affects the viscosity in a substantial way. In a viscometer, when $Na/Wi^2 = h^2 G^2 \beta / \mu k > 1$ thermal softening will overwhelm the shear-dependence of viscosity; however if $Na/Wi^2 < 1$, it still cannot be said that thermal softening will not be important at any magnitude of shear. Note that this combined group, Na/Wi^2, does not depend on the film thickness or kinematics; it only depends on the liquid properties at the local temperature *T* and pressure *p*. In this work the Nahme-Griffith number will be evaluated at the contact center.

4.3 Limiting-Shear-Stress Number

A new dimensionless number is proposed here to allow the prediction of the onset and offset of Limiting-Shear-Stress. This number shall be called *Li* and is defined as follows:

$$Li = \frac{\tau_u}{\tau_L} = \frac{\tau_u}{\Lambda\ p} \qquad (16)$$

Where τ_u corresponds to the unbounded value of the shear stress τ, that is the value of the shear stress that would be obtained when the LSS is switched off (no truncation). Therefore, *Li* can be used to predict the onset and offset of limiting-shear-stress by simply comparing its value to unity. When $Li > 1$, it can be said that the limiting-shear-stress regime is reached and the greater the value of *Li* compared to unity, the greater the truncation in the value of the shear stress τ. In this work *Li* will be evaluated at the contact center.

4.4 Roller Compliance Number

For very high contact pressure combined with low slide-to-roll ratio, Σ, the friction is linear with Σ and the friction is indistinguishable from the friction in dry, unlubricated contact [24]. The thin liquid film has become stiffer in shear than the overall elastic compliance of the rollers and the surface velocity difference far from the contact patch is dominated by the elastic creep of the rollers [25]. Under these conditions the friction coefficient is simply $f = \Sigma\left(G_S / p_h\right)$, where G_S is the shear modulus of the roller material and p_h is the maximum Hertz pressure. Define a roller elasticity number as

$$Er = \frac{p_h f}{\Sigma G_s} \qquad (17)$$

Large values of *Er* lead to the roller compliance contributing more to the velocity difference calculated from the rotational speeds of the rollers than does the liquid shear. For large *Er*, the friction calculation must include the roller elasticity component of the velocity difference.

5. Results

In this section, a series of numerical tests are run over a wide range of operating conditions. All tests correspond to steel-steel ball-on-plane circular contacts lubricated with Shell T9 lubricant. The ball radius is taken to be R=12.7mm. The lubricant transport properties are assumed to vary according to the models described in section 2. Three categories of loads are considered: Low, Moderate and High loads. In the Low load category, one loading condition is considered in which the external applied load is F=25N corresponding to a Hertzian pressure p_h=0.74 GPa. In the Moderate load category, two external loads are considered 50N and 100N corresponding to Hertzian contact pressures of 0.93GPa and 1.17GPa respectively. And finally, for the High load category, only one loading condition is considered with F=200N corresponding to a Hertzian contact pressure p_h=1.47GPa. For all considered loads, mean entrainment speeds U_m are varied in the range of 0.5 - 10.0 m/s with Slide-to Roll Ratios Σ ranging from 0 to 0.5. The operating conditions and solid material properties are summarized in Table 1 where the inlet reciprocal isoviscous pressure denotes the pressure-viscosity coefficient according to [8].

Property	Value
Inlet temperature	30°C
Inlet viscosity	0.0135 Pa.s
Inlet reciprocal isoviscous pressure [8]	20.25 GPa^{-1}
Mean Entrainment Speed	0.5-10 m/s
Slide-to-Roll Ratio	0.0001-0.5
External Applied Load	25, 50, 100, 200N
Ball Radius	12.7 mm
Steel Young's Modulus	210 GPa
Steel Poisson Coefficient	0.3

Table 1: Operating conditions and solid material properties

Typical traction curves are shown in Figures 1, 2 and 3 for all three load categories low, moderate and high respectively. In each figure, two typical mean entrainment speeds U_m are considered (moderate and high) and traction curves are shown for all four types of numerical tests: "Full Potential", "Thermal Off", "LSS Off" and "Shear-Thinning Off". Note that the "Full Potential" results correspond to the realistic traction curves that were validated against experiments in a previous work [12].

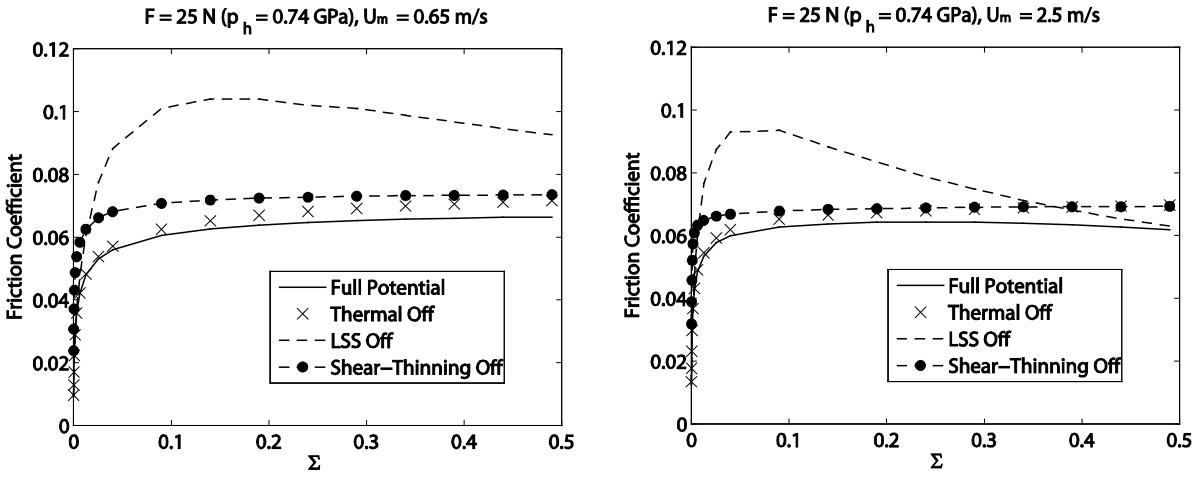

Figure 1: Traction curves under low load conditions (F=25N, p_h=0.74GPa and Left:U_m=0.65m/s, Right: U_m=2.5m/s)

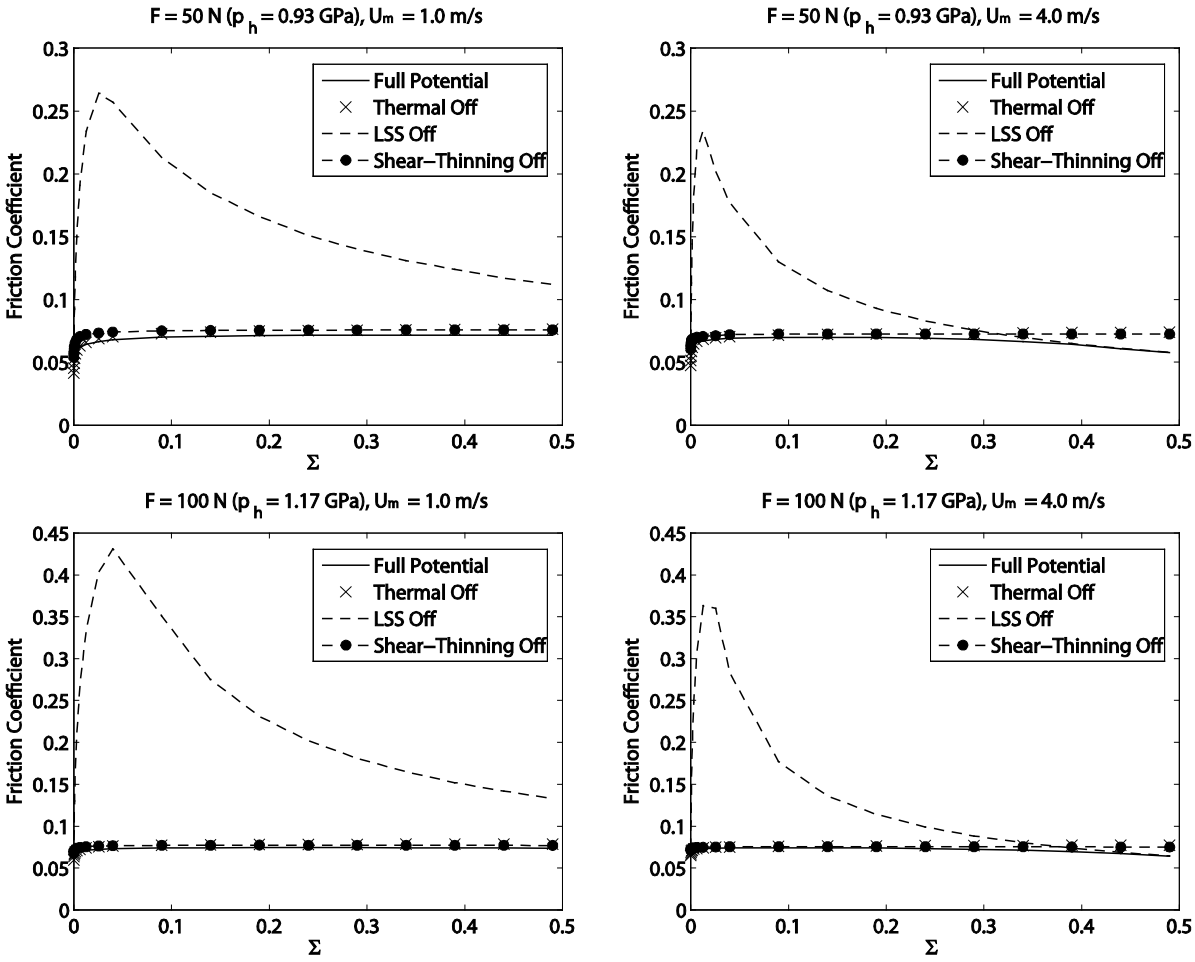

Figure 2: Traction curves under moderate load conditions (Up: F=50N, p_h=0.93GPa, Down: F=100N, p_h=1.17GPa, and Left: U_m=1.0m/s, Right: U_m=4.0m/s)

It is clear from Figures 1, 2 and 3 that Limiting-Shear-Stress is the most important factor to include in traction calculations at moderate to high loads. When not considered (LSS Off), traction predictions become less and less realistic with increasing loads. This is only true when considering sufficiently high loads and speeds such that the Limiting-Shear-Stress is actually reached inside the lubricant film. However, if operating conditions are such that Limiting-Shear-Stress is not actually reached, the latter will be of no importance for friction prediction as can be seen in Figure 4 which shows traction curves for a very low load and a relatively low mean entrainment speed. It is clear that under such regime, ignoring the Limiting-Shear-Stress has no effect and the "Full Potential" and "LSS Off" traction curves fully overlap. Clearly, thermal effects have also little importance under such conditions; however, it is shear-thinning that dominates the frictional behavior of the contact and failing to consider it would lead to totally erroneous predictions.

It can also be noted from Figures 1, 2 and 3 that under sufficiently high loads, in the high Σ regime, traction behavior is dominated by thermal and sometimes shear-thinning effects. These can even overwhelm Limiting-Shear-Stress effects and it can be seen that even when limiting stress is not considered, friction predictions can be accurate at high sliding provided that thermal and shear-thinning effects are considered. As a matter of fact, the "LSS Off" and "Full Potential" curves overlap for the high mean entrainment speed cases at high Σ.

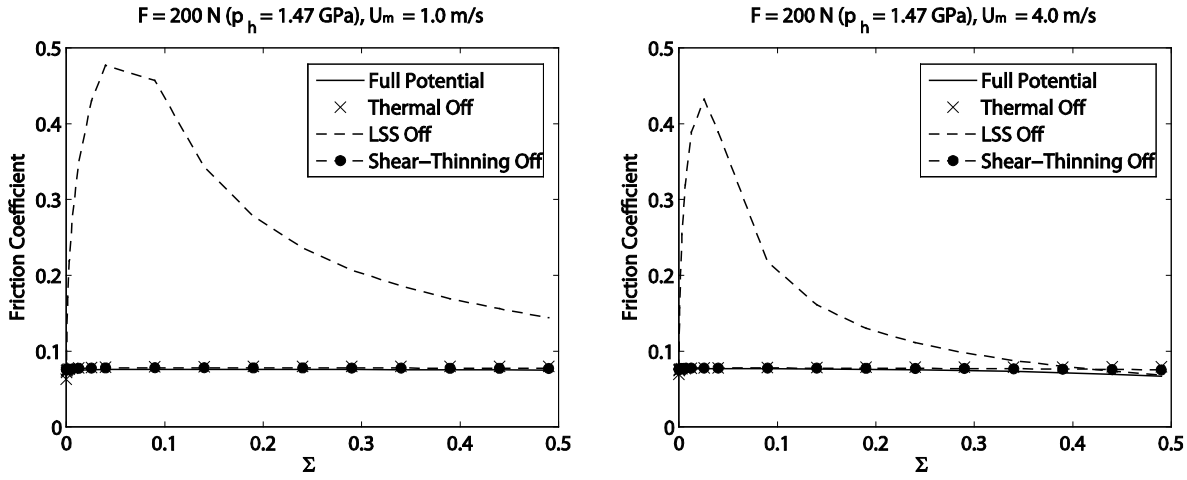

Figure 3: Traction curves under high load conditions (F=200N, p_h=1.47GPa and Left:U_m=1.0m/s, Right: U_m=4.0m/s)

Hence, one can say that when LSS is reached it dominates the frictional response of the contact until combined thermal and shear-thinning effects become more important (at high Σ). And under moderate Σ, both shear-thinning and thermal effects have little importance. However, for low loads (See Figure 1), even when LSS is reached shear-thinning can be said to still have a significant impact on the frictional response of EHL contacts. Since LSS is normally reached first in the central area of the contact, this indicates that it is the shear-thinning occurring in the peripheral area of the contact that is acting on reducing friction.

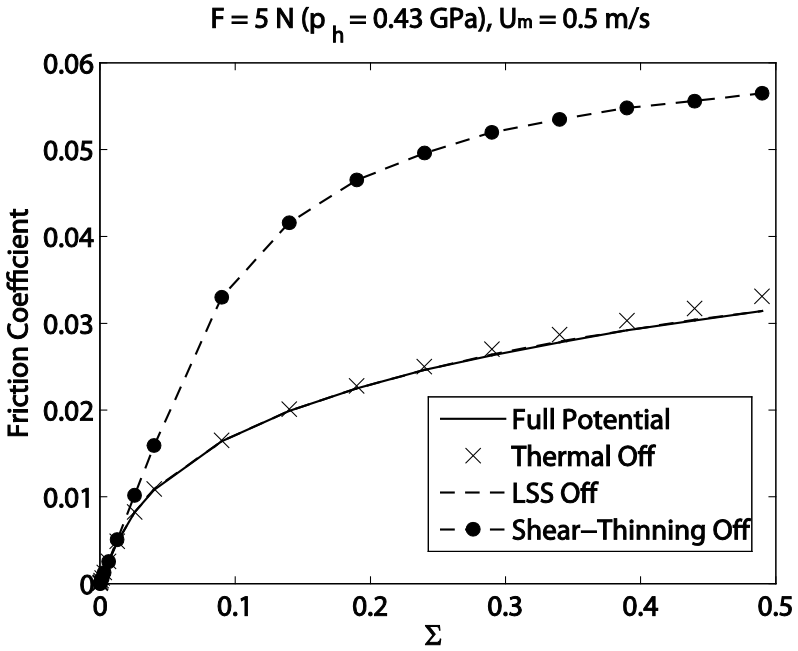

Figure 4: Traction curves under very low loading and low speed conditions (F=5N, p_h=0.43GPa and U_m=0.5m/s)

To summarize and clarify all observations made so far in this section the reader is referred to the flow chart of Figure 5 which highlights the main features and regimes encountered in EHL traction curves.

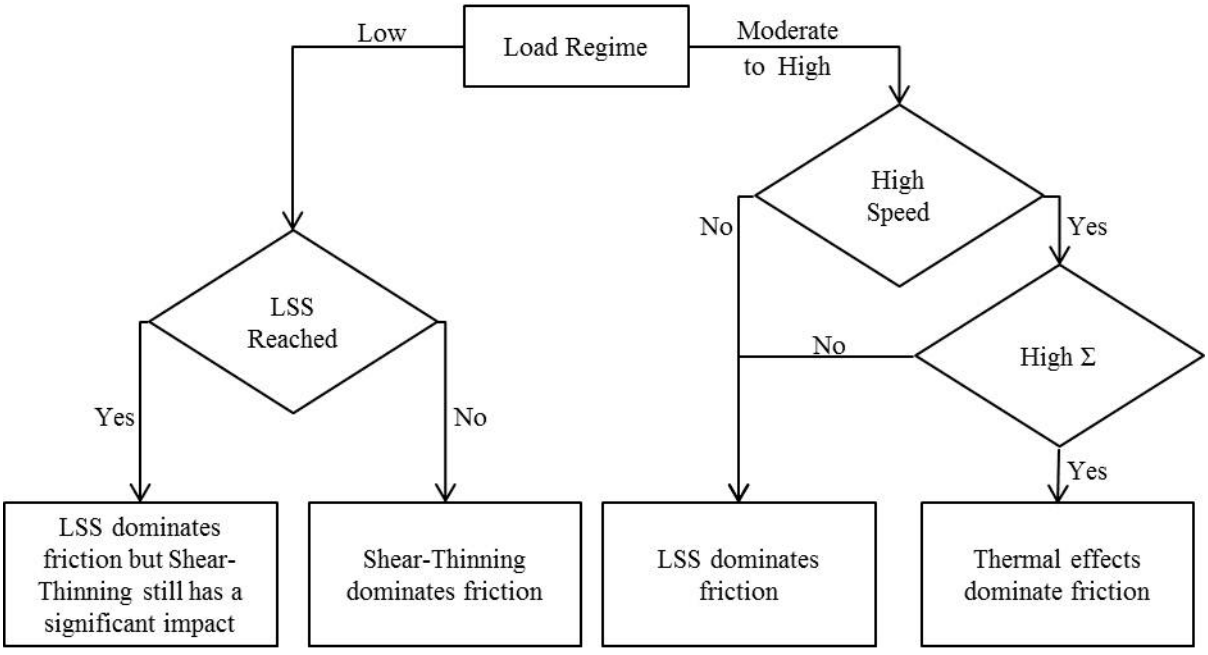

Figure 5: Flow chart of dominant parameters in frictional response of EHL contacts

Note that for all loading and speed conditions; the first part of any traction curve is linear with Σ, indicating Newtonian response of the lubricant at very low Σ and low pressure and indicating roller elastic compliance for very high pressure. The elastic compliance of the rollers

is neglected in the simulations. The effect of roller compliance can be observed by comparing dry and lubricated traction at small Σ. Elastic response of the liquid may be neglected since the film is thin and the shear modulus of the liquid is of the order of GPa.

6. Traction Regimes

It must be made clear that it is impossible to fully identify discrete regimes on the basis of the visual inspection of a traction curve and many misleading conclusions have been drawn from this technique in the past. Based on the traction results discussed so far, it is clear that four different traction regimes might be encountered in any traction curve based on the operating conditions. These regimes are:

1- **Linear Regime:** Friction varies linearly against Σ indicating that the frictional response of the contact is governed by the Newtonian viscous behavior of the lubricant.

2- **Non-Linear Viscous Regime:** Friction departs from linear behavior indicating that shear-thinning and/or thermal dissipation and/or limiting shear stress behavior of the lubricant are affecting the frictional response of the contact.

3- **Plateau Regime:** Friction reaches an asymptotic value and shows little variation indicating that the frictional response of the contact is governed by the limiting-shear-stress behavior of the lubricant.

4- **Thermoviscous Regime:** Friction decreases with increasing sliding speeds, indicating that both thermal dissipation and shear-thinning effects are governing the frictional response of the contact and overwhelming all other effects including LSS.

In addition, one could have also defined a second linear regime at high pressure and very low Σ which supersedes the Newtonian viscous one. In this regime, the frictional response of the contact is governed by the elastic properties of the contacting solids rather than the lubricant rheological behavior (See Appendix for more details). Note that all regimes are not necessarily encountered together in any traction curve. Depending on the operating conditions, one might be able to identify one, two or three different traction regimes only in a single traction curve. Identification of the different traction regimes encountered in EHL contacts has nothing new in itself and these regimes are more or less commonly accepted by the scientific community. However, what lacks in the literature is a quantitative identification of these regimes. That is, a quantitative link between these regimes and the different dimensionless numbers defined in section 4. It would be of significant importance to identify clear ranges of these dimensionless numbers where each regime is encountered. Next, the authors attempt to fill this gap for the four different traction regimes discussed in this section.

Remark: In the following, all dimensionless numbers are evaluated at the center of the contact in the mid-plane of the lubricant film using actual values of temperature, pressure, viscosity, shear stress, etc. obtained from the numerical solution.

6.1 Linear Regime

In section 4, the Weissenberg number *Wi* was recalled. When this number exceeds unity, shear-thinning is occurring within a given fluid. Therefore, while this number is less than unity a linear friction response should be expected within an EHL contact. Thus the condition for occurrence of the linear regime is:

$$\text{Linear Regime:} \quad Wi < 1 \qquad (18)$$

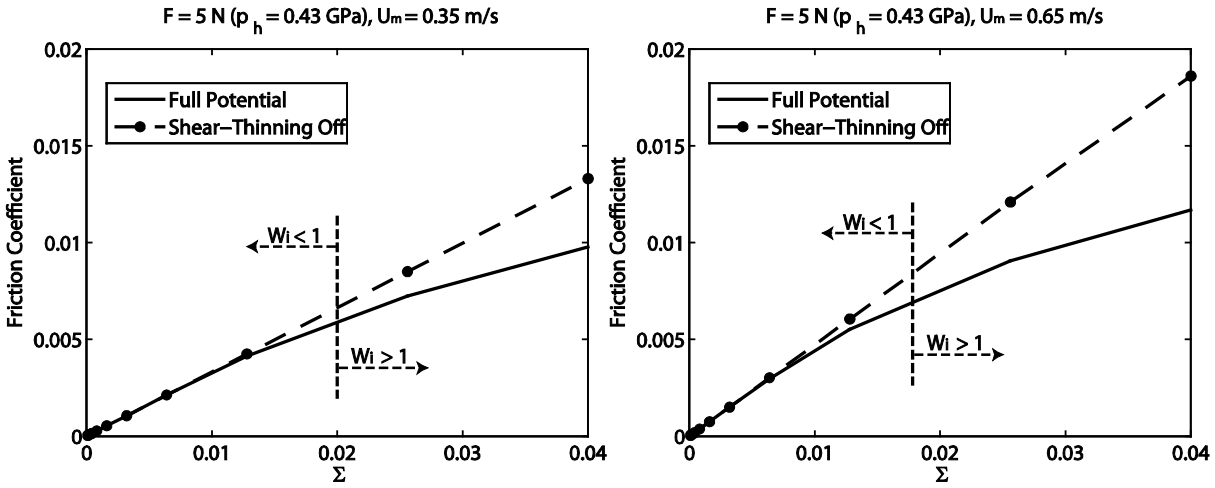

Figure 6: Delimitation of the linear traction regime using the Weissenberg dimensionless number

To verify this condition, Figure 6 shows the traction curves for the 5N loading case for two different mean entrainment speeds (0.35 and 0.65 m/s). It is clear that when $Wi < 1$, the "Shear-Thinning-Off" curve coincides with the "Full-Potential" one, indicating that shear-thinning effects are non-existent. Besides, the traction curves are linear against Σ under these conditions. In the interest of completeness, it must be mentioned that at high pressure and very low slide-to-roll ratio there is another linear regime which will be briefly discussed in a following section.

6.2 Non-Linear Viscous Regime

It is clear from the previous section that shear-thinning and thus the Non-Linear traction regime starts when $Wi > 1$. Thus, shear-thinning is expected to dominate the frictional response of the contact until limiting-shear-stress is reached, that is until $Li = 1$. This being said, the condition for occurrence of the Non-Linear Viscous regime reads:

$$\text{Non-Linear Viscous Regime:} \quad Wi > 1 \quad \& \quad Li < 1 \qquad (19)$$

This condition might not be sufficiently general at this point as will be detailed in section 6.4.

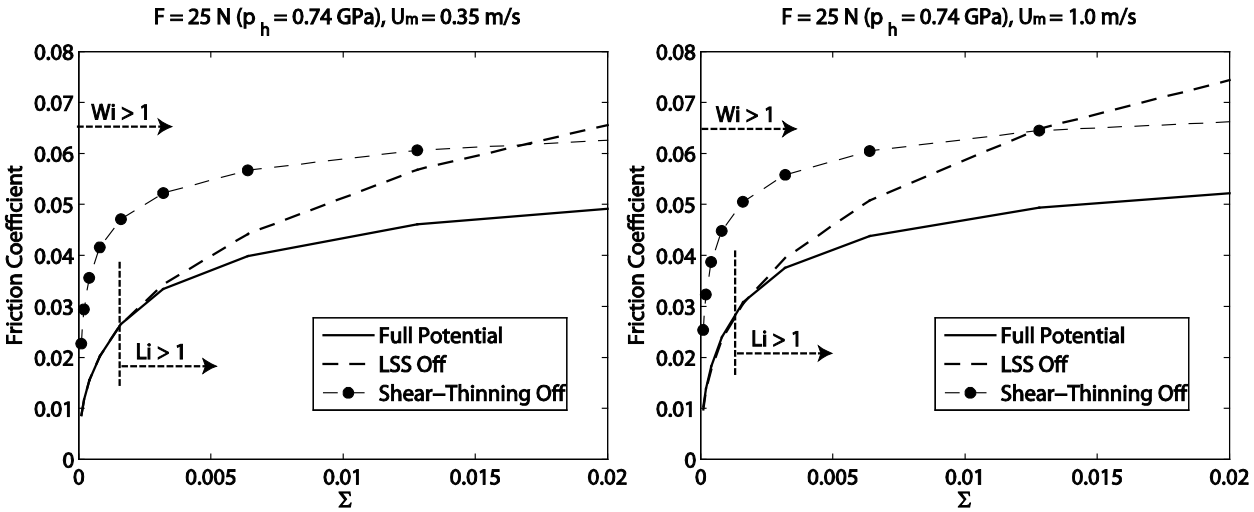

Figure 7: Delimitation of the non-linear viscous traction regime using the Weissenberg and Limiting-Shear-Stress dimensionless numbers

Figure 7 shows the traction curves for the 25N loading case for two different mean entrainment speeds (0.35 and 1.0 m/s). For the sake of simplicity, the "Thermal Off" curve has been removed as it perfectly coincides with the "Full Potential" one under these conditions. Note that for $Li > 1$, the "LSS Off" curve deviates from the "Full Potential" one indicating that limiting-shear-stress has been reached and started affecting the frictional response of the contact. It is important to note that $Wi > 1$ for all values of Σ, and these curves do not show any linear response even at the smallest Σ considered here ($\Sigma = 10^{-4}$). And until limiting-shear-stress is reached ($Li = 1$) it can be said that shear-thinning effects dominate the frictional response of the contact. Failing to consider these leads to an inaccurate estimation of friction. More importantly, note that, contrarily to what is commonly believed, the limiting-shear-stress and the friction plateau are not necessarily reached simultaneously. The plateau starts for $Li \gg 1$, and even when it starts, shear-thinning still affects the frictional response of the contact. Since limiting-shear-stress is first reached in the central area of the contact, this indicates that shear-thinning occurring in the peripheral area of the contact still affects its frictional response. This explains the gap between the "Shear-Thinning Off" and "Full Potential" traction curves even after the friction plateau is reached.

6.3 Plateau regime

It is clear from the previous section that the Plateau regime, characterized by a friction plateau, is reached for $Li >> 1$. From the numerical experiments of the current work, it is found that a value of $Li = 2$ is suitable to define the onset of the Plateau regime. The latter persists until thermal and shear-thinning effects dominate the frictional response of the contact and overwhelm limiting-shear stress effects. In fact, Figure 8 (Right) suggests that at high sliding speeds, the plateau disappears and friction begins to decrease. It is widely believed in the tribological community that this is due to the dominance of thermal effects on friction. It is true

that the negative slope observed in traction curves at high Σ can be attributed to thermal effects as isothermal traction curves never reveal such a trend. However, examining Figure 8 (Right) closely suggests that the extent of decrease in the friction coefficient cannot be simply attributed to thermal effects, but also to shear-thinning. In fact, both the "Shear-Thinning Off" and "Thermal Off" curves deviate from the "Full Potential" one at high sliding speeds suggesting that both shear-thinning and thermal effects are affecting the frictional response of the contact. This being said, the Plateau regime should be delimited on the left side using the Limiting-Shear-Stress dimensionless number *Li*, and on the right side by the disappearance of the friction plateau highlighted by a decrease in friction. The latter is expected to be observed when both shear-thinning and thermal dissipation overwhelm limiting-shear-stress, in other words, when $Na \times Wi$ becomes much greater than *Li*. Consider a new dimensionless number *Ti* that can be used as a thermoviscous regime indicator and defined as:

$$Ti = \frac{Na \times Wi}{Li} \qquad (20)$$

Therefore, the condition for occurrence of the Plateau regime can be defined as a function of *Li* and *Ti* as follows:

$$\text{Plateau Regime:} \quad Li > 2 \quad \& \quad Ti < 100 \qquad (21)$$

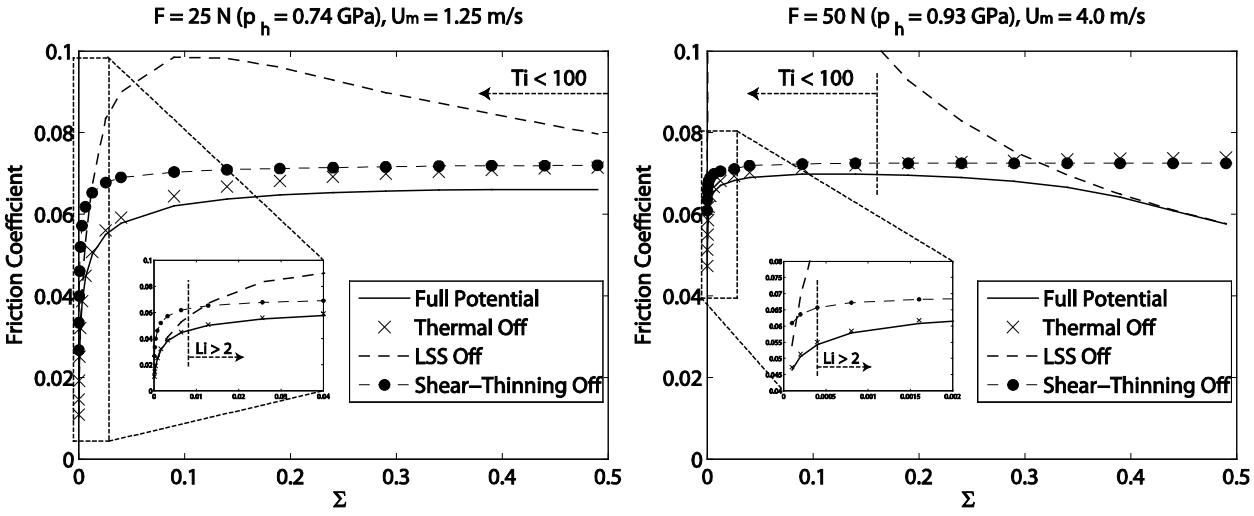

Figure 8: Delimitation of the limiting traction regime using the Nahme-Griffith and Limiting-Shear-Stress dimensionless numbers

The condition established in equation (21) for delimiting the Plateau traction regime is confirmed by observing Figure 8. The latter suggests that for both cases considered (25N – 1.25m/s and 50N – 4.0m/s), the friction plateau is delimited from the left side by $Li = 2$ and from the right side by $Ti = 100$. Note that for the 25N case (Figure 8, left) the entire traction curves fall within the range $Ti < 100$, this is why no decrease in friction is observed at high sliding speeds.

6.4 Thermoviscous Regime

Finally, the thermoviscous traction regime, characterized by a decrease in friction at high sliding speeds can be delimited by simply using the newly proposed dimensionless number *Ti* and the condition for occurrence of this regime can be written as:

$$\text{Thermoviscous Regime:} \quad Ti > 100 \qquad (22)$$

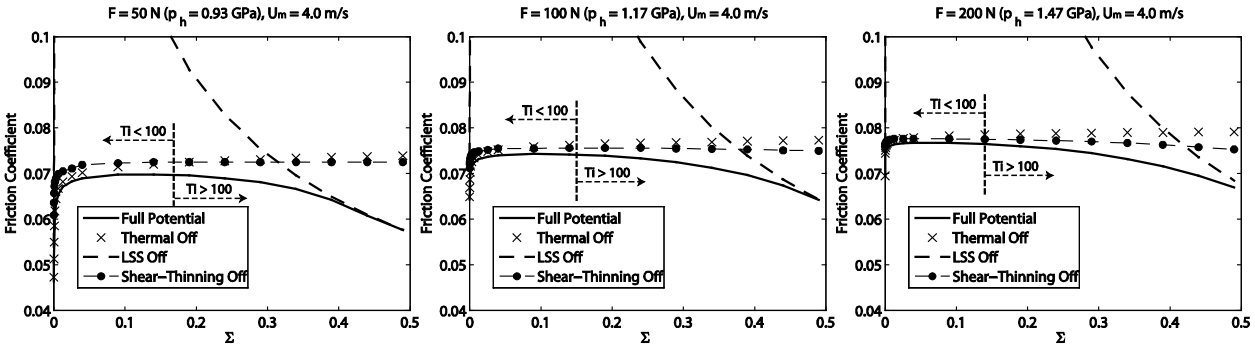

Figure 9: Delimitation of the thermoviscous traction regime using the dimensionless number *Ti*

Figure 9 clearly confirms the condition defined in equation (22) for delimiting the thermoviscous traction regime. In fact, it is clear for all three considered loads (50, 100 and 200N) that friction starts decreasing whenever *Ti* exceeds 100. Also note that at very high sliding speeds, the "LSS Off" and "Full Potential" curves overlap indicating that shear-thinning and thermal effects completely dominate the frictional response of the contact overwhelming limiting-shear-stress effects which vanish. In fact, thermal dissipation and shear-thinning both act on decreasing viscosity at high sliding speeds to an extent that the limiting-shear-stress behavior of the lubricant is no longer reached. This being said, *Li* would be less than unity and equation (19) would have to be updated to:

$$\text{Non-Linear Viscous Regime:} \quad Wi > 1 \quad \& \quad Li < 1 \quad \& \quad Ti < 100 \qquad (23)$$

7. Conclusion

This paper identifies the different friction regimes encountered in elastohydrodynamic lubricated point contacts using a quantitative, physics-based approach. The idea is to link different traction regimes to dimensionless numbers and identify ranges of those numbers where a given regime is encountered or dominates the friction response of the contact. For this, a set of well-known dimensionless numbers is used in combination with a set of newly developed ones. A numerical investigation of traction in point contacts lubricated with a typical mineral oil is employed. The measured thermo-physical properties of the oil are used without any modification to force agreement with experiments. The authors propose four friction regimes:

1- **Linear Regime:** Friction varies linearly against Σ indicating that the frictional response of the contact is governed by the Newtonian viscous behavior of the lubricant.

2- **Non-Linear Viscous Regime:** Friction departs from linear behavior indicating that shear-thinning and/or thermal dissipation and/or limiting shear stress behavior of the lubricant are affecting the frictional response of the contact.

3- **Plateau Regime:** Friction reaches an asymptotic value and shows little variation indicating that the frictional response of the contact is governed by the limiting-shear-stress behavior of the lubricant.

4- **Thermoviscous Regime:** Friction decreases with increasing sliding speeds, indicating that both thermal dissipation and shear-thinning effects are governing the frictional response of the contact and overwhelming all other effects including LSS.

The four regimes are delimited by the combined values of three dimensionless parameters as summarized by the flow chart of Figure 10.

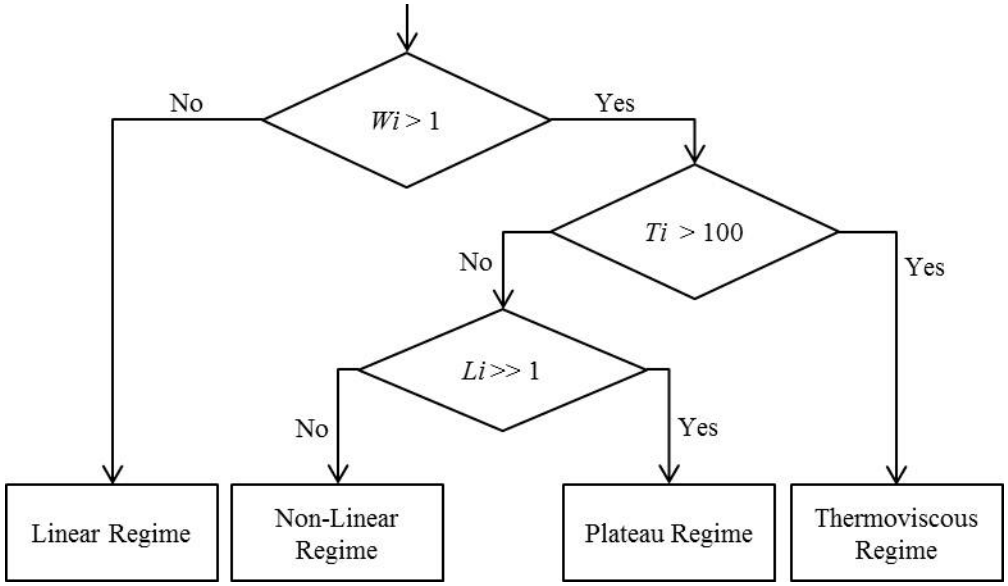

Figure 10: Flow chart for quantitative delineation of friction regimes

This work clearly emphasizes the necessity of using actual measured physical properties of liquids for a better understanding of traction in EHL contacts. Many interesting conclusions and observations can be drawn from this study:

1- Even when limiting-shear-stress is reached, shear-thinning can be said to still have a significant impact on the frictional response of EHL contacts. Since LSS is normally reached first in the central area of the contact, this indicates that it is the shear-thinning occurring in the peripheral area of the contact that acts on reducing friction.

2- The previous point clearly suggests that, contrarily to what is commonly believed, the limiting-shear-stress and the friction plateau are not necessarily reached simultaneously. The plateau starts well after the limiting-shear-stress is reached, and until it starts, shear-thinning still affects the frictional response of the contact. This being said, the value of the limiting-

stress pressure coefficient Λ cannot necessarily be accurately deduced from the value of the friction coefficient f along the plateau, which is the current common practice in EHL. A value from a rheometer that can demonstrate rate-independent shear would be more reliable.

3- Contrarily to what is commonly believed, at high slide-to-roll ratios, when the friction coefficient begins to decrease with increasing Σ, the extent of the friction decrease cannot be attributed to the dominance of thermal effects alone. Shear-thinning plays an equally important role in reducing friction in the thermoviscous regime.

Finally, in this work, owing to the scarcity of reliable lubricant transport properties modeling under EHL conditions, only one lubricant has been used to delineate the four proposed traction regimes. However, it would be interesting in the future, when more lubricants are sufficiently well characterized (with the same level of accuracy as Shell T9) to apply the proposed approach to a wider variety of lubricants and verify its validity.

Appendix: Discussion on Very Low Σ Traction

In the interest of completeness, it must be mentioned that at high pressure and very low slide-to-roll ratio there is another linear regime which will supersede the Newtonian viscous one [24][25]. The elastic creep of the rollers was not addressed in the present numerical work but may be introduced with experimental measurements.

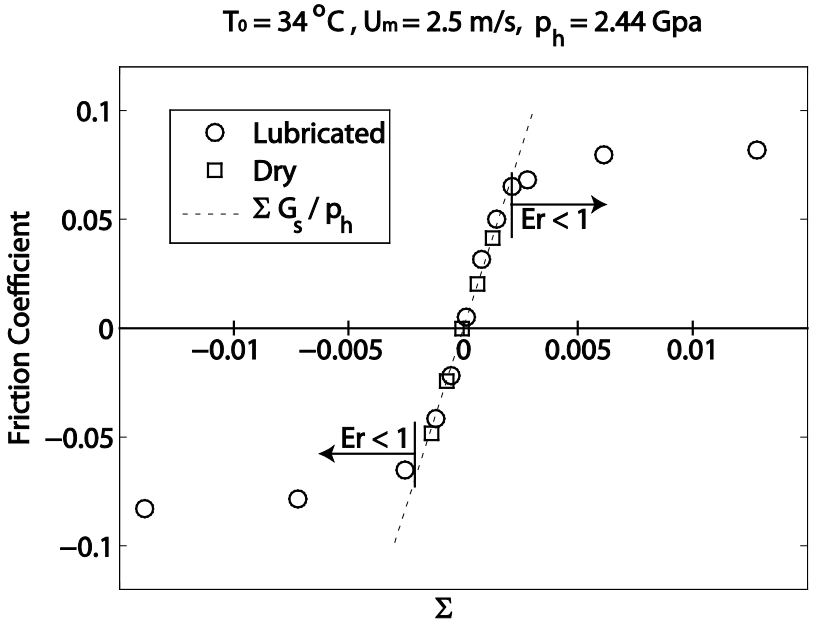

Figure 11: Traction measured for T9 at very low slide-to-roll ratio in a crossed roller instrument

Experimental investigations of traction for $\Sigma < 1\times10^{-3}$ find that the response is linear with a slope equal to the slope measured for dry contact [25]. See Figure 11 where measurements of both dry and lubricated traction follow the same linear slope with friction coefficient, f, equal to $\Sigma G_s / p_h$ for small values of Σ delimited by the relation, $E_r > 1$. Failure to recognize that roller

elastic creep can influence the traction curve has resulted in the assignment of reduced high-pressure viscosity or high-frequency shear modulus of the liquid to explain this regime going back to the earliest contributions [2].

Nomenclature

η : Lubricant's Generalized Newtonian viscosity
Σ : Slide-to-Roll ratio $=(V_1-V_2)/U_m$
μ : Lubricant's viscosity
μ_∞ : Lubricant's viscosity extrapolated to infinite temperature
ρ : Lubricant's density
ρ_R : Lubricant's density at reference state
Λ : Limiting stress-pressure coefficient
τ : Shear stress
τ_L : Limiting shear stress
τ_u : Unbounded shear stress
Ti : Thermoviscous indicator dimensionless number
c : Lubricant's heat capacity
C : Lubricant's volumetric heat capacity
Er : Roller elasticity number
f : Friction coefficient
F : Contact external applied load
G : Lubricant effective shear modulus
G_s : Roller material shear modulus
h : Lubricant film thickness
k : Lubricant's thermal conductivity
Li : Limiting-shear-stress dimensionless number
Na : Nahme-Griffith dimensionless
p : Pressure
p_h : Hertzian contact pressure
p_0 : Ambient pressure
p_R : Reference pressure
T : Temperature
T_0 : Ambient temperature
T_R : Reference temperature
U_m : Mean entrainment speed $=(V_1+V_2)/2$
V_1 : Sphere's surface velocity
V_2 : Plane's surface velocity
V : Volume
V_R : Volume at reference state
Wi : Weissenberg dimensionless number

Acknowledgments

The first author wishes to thank the Council for International Exchange of Scholars (CIES) and the Fullbright commission for funding his visiting scholar program at the Georgia Institute of Technology. Bair was supported by the Center for Compact and Efficient Fluid Power, a National Science Foundation Engineering Research Center funded under cooperative agreement number EEC-0540834.

References

[1] Smith, F.W. "Lubricant Behavior in Concentrated Contact-Some Rheological Problems", *ASLE Transactions*, Vol.3, No.1, 1960, pp. 18-25.

[2] Crook, A.W., "The Lubrication of Rollers IV. Measurements of Friction and Effective Viscosity", *Phil. Trans. Roy. Soc. Lond.*, Series A, Vol. 255, No. 1056, 1963, pp. 281-312.

[3] Bell, J.C., "Lubrication of Rolling Surfaces by a Ree-Eyring Fluid," *ASLE Transactions*, Vol. 5, 1962, pp. 160-171.

[4] Johnson, K.L. and Tevaarwerk, J.L., "Shear Behaviour of Elastohydrodynamic Oil Films", *Proc. Roy. Soc. London* A, Vol.356, 1977, pp. 215-236.

[5] Hirst, W. and Moore, A.J., "The Effect of Temperature on Traction in Elastohydrodynamic Lubrication", *Phil. Trans. Royal Soc. London* A, Vol.298, No.1438, 1980, pp.183-208.

[6] Jacod B., Venner C. H. and Lugt P. M., "A Generalized Traction Curve for EHL Contacts", *ASME Journal of Tribology*, 2001, vol. 123, pp. 248-253.

[7] Bair S. – High Pressure Rheology for Quantitative Elastohydrodynamics, Elsevier Science, Amsterdam, 2007.

[8] Bair S. – Reference Liquids for Quantitative Elastohydrodynamics: Selection and Rheological Characterization, *Tribology Letters*, 2006, vol. 22, pp. 197-206.

[9] Kumar P. and Khonsari M. M. – Combined Effects of Shear-Thinning and Viscous Heating on EHL Characteristics of Rolling-Sliding Line Contacts, *ASME Journal of Tribology*, 2008, vol. 130, doi: 10.1115/1.2959111.

[10] Liu Y., Jane Wang Q., Bair S. and Vergne P. – A Quantitative Solution for the Full Shear-Thinning EHL Point Contact Problem Including Traction, *Tribology Letters*, 2007, vol. 28, pp. 171-181.

[11] Habchi. W., Eyheramendy D., Bair S., Vergne P. and Morales-Espejel G. – Thermal Elastohydrodynamic Lubrication of Point Contacts Using a Newtonian / Generalized Newtonian Lubricant, *Tribology Letters*, 2008, vol. 30 (1), pp. 41-52.

[12] Habchi W., Vergne P., Bair S., Andersson O., Eyheramendy D. and Morales-Espejel G. E. – Influence of Pressure and Temperature Dependence of Thermal Properties of a Lubricant on the Behaviour of Circular TEHD Contacts, *Tribology International*, 2010, vol. 43, pp. 1842-1850.

[13] Habchi W., Vergne P., Fillot N., Bair S. and Morales-Espejel G. E. – A Numerical Investigation of Local Effects on the Global Behavior of TEHD Highly Loaded Circular Contacts, *Tribology International*, 2011, vol. 44, pp. 1987-1996.

[14] Evans, C.R. and Johnson, K.L., "Regimes of Traction in Elastohydrodynamic Lubrication," Proceedings of the Institution of Mechanical Engineers, Part C: Journal of Mechanical Engineering Science, 1986, vol. 200 no. 5, pp. 313-324.

[15] Murnaghan, F.D., 1944, “The Compressibility of Media under Extreme Pressures”, Proceedings of the National Academy of Sciences, Vol. 30, p. 244-247.

[16] Vogel H. – The Temperature Dependence Law of the Viscosity of Fluids, *Physikalische Zeitschrift*, 1921, vol. 22, pp. 645-646.

[17] Bair, S., 2004, “A Rough Shear Thinning Correction for EHD Film Thickness”, *STLE Tribology Trans*., Vol. 47, N°3, p. 361-365.

[18] Habchi W., Eyheramendy D., Vergne P. and Morales-Espejel G. – Stabilized Fully-Coupled Finite Elements for Elastohydrodynamic Lubrication Problems, *Advances in Engineering Software*, 2012, vol. 46, pp. 4-18.

[19] Yang, P., Wen, S. - A Generalized Reynolds Equation for Non-Newtonian Thermal Elastohydrodynamic Lubrication, *ASME J. Tribol.*, 1990, vol. 112, pp. 631-636.

[20] Wu S. R. – A Penalty Formulation and Numerical Approximation of the Reynolds-Hertz Problem of Elastohydrodynamic Lubrication. *Int. J. Engnrng. Sci.*, 1986, vol. 24 (6), pp. 1001-1013.

[21] Deuflhard P. – Newton Methods for Nonlinear Problems, Affine Invariance and Adaptive Algorithms. *Springer*, Germany, 2004.

[22] Bird R. B., Armstrong R. C. and Hassager O. - Dynamics of Polymeric Liquids, Vol.: 1 Fluid Mechanics, second edition, *Wiley*, New York, 1987, p 94.

[23] Winter H. H. - Viscous Dissipation in Shear Flows of Molten Polymers, *Advances in Heat Transfer*, Vol. 13, 1977, pp205-267

[24] Bair, S. and Kotzalas, M., “The Contribution of Roller Compliance to Elastohydrodynamic Traction”, STLE *Tribology Trans*., Vol.49, No.2, 2006, pp.218-224.

[25] Kalker, J.J., *On the Rolling Contact of Two Elastic Bodies in the Presence of Dry Friction*, Dr.-Ing Thesis, TLT Delft, 1967, pp. 90-95.